THE JOURNAL OF PHYSICAL CHEMISTRY C

Article

pubs.acs.org/JPCC

Quantum State Resolved 3D Velocity Map Imaging of Surface-Scattered Molecules: Incident Energy Effects in HCl + Self-Assembled Monolayer Collisions

Carl H. Hoffman and David J. Nesbitt*

Department of Chemistry and Biochemistry, University of Colorado, and JILA, National Institute of Standards and Technology, Boulder, Colorado 80309-0440, United States

ABSTRACT: Thermal and hyperthermal HCl ($v = 0$, $J = 0$) collision dynamics at the surface of methyl-terminated self-assembled monolayers (SAMs) are probed by state-selective ionization followed by velocity-map imaging (VMI) to yield a full 2π steradian map of final 3D velocity distributions (v_x, v_y, v_z) as a function of rovibrational (v, J) quantum state. "DC slicing" of the scattered HCl flux normal to the surface (v_z) provides a powerful tool for eliminating incident beam contamination, as well as access to fully correlated, 3D flux weighted rovibrational quantum state + translational scattering dynamics in unprecedented detail. At low collision energies ($E_{inc} \approx 0.7(1)$ kcal/mol), the scattering dynamics are completely dominated by trapping-desorption (TD) events, for which both external (i.e., translational) and internal (i.e., rovibrational) degrees of freedom quantitatively track the SAM surface temperature (T_S). Hyperthermal scattering data at high collision energies ($E_{inc} \approx 17(1)$ kcal/mol) provide direct evidence for growth of an additional nonequilibrium, impulsive scattering (IS) channel, with a strong forward scattering propensity broadly distributed around the specular angle. The competition between linear and angular momentum transfer for such a rapidly rotating hydride species ($B_{HCl} \approx 10$ cm^{-1}) is investigated in the IS channel, which reveals strong retention of translational energy with only modest rotational excitation ($\kappa_{trans} \approx 48(7)\%$, $\kappa_{rot} \approx 6(2)\%$) and in clear contrast with studies of more slowly tumbling species ($B_{CO2} \approx 0.4$ cm^{-1}) such as CO_2 ($\kappa_{trans} \approx 6(2)\%$, $\kappa_{rot} \approx 20(4)\%$). Most importantly, the combination of (i) full 2π steradian angular data with (ii) full quantum state resolution permits a model free deconstruction of the experimental velocity map images into TD and IS components, which provides striking, independent confirmation of the hyperthermal yet Boltzmann-like nature of both the (i) IS quantum state and the (ii) out-of-plane momentum distributions. In summary, this novel combination of VMI with quantum state resolved scattering techniques provides powerful synergistic opportunities for correlated investigation of quantum state resolved reactive and inelastic energy transfer dynamics at gas−liquid-like interfaces with chemically "tunable" surface moieties.

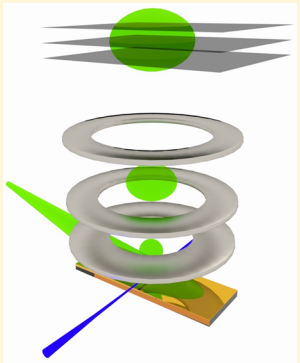

I. INTRODUCTION

The early steps of the interaction between gas and condensed phase reactants are of critical importance in any surface chemical reaction dynamics, which may then proceed to either (i) react and desorb, (ii) thermalize with the surface, or (iii) dissolve into the bulk. Such inelastic and reactive scattering processes are involved in nearly every branch of chemistry, with particular relevance to terrestrial/extraterrestrial molecular collisions with ice/dust particles,[1−5] etching of spacecraft surfaces during reentry,[6−9] catalysis,[10−13] and the dynamics of atmospheric gas−aerosol[14] and gas−liquid reactions.[15,16] The search for understanding of these complex, branching processes has led to the development of many sensitive measurement techniques to study surface geometry and composition, such as reflection−absorption infrared spectroscopy[17,18] and sum-frequency generation,[10,19,20] as well as to probe dynamics and reactivity with molecular beams via time-of-flight mass spectroscopy,[6−8,15,21−26] direct absorption spectroscopy,[27−31] and laser-induced fluorescence.[32−35]

These molecular beam scattering experiments in particular have proven to be a rich source of dynamical insights, specifically identifying a robust and remarkably simple paradigm for nonreactive scattering by way of two qualitatively different channels.[36−38] In the context of such a "microscopic branching" picture, the incident molecules either (i) stick to the surface, thermally equilibrate, and eventually desorb (i.e., the trapping-desorption or TD channel), or (ii) promptly leave the surface after only a relatively few gas−surface interactions (i.e., the impulsive scattering or IS channel). The TD channel offers information on a surface's ability to absorb energy from and thereby trap incident projectile molecules with various speeds, angles, and internal states, and thereby provide a measure of the surface softness or roughness.[27] The IS channel, on the other hand, retains some memory of the molecule's incident velocity and internal quantum state, and the ways in which these properties change during the collision give information about the torques, forces, and molecular orientations involved. These laser-based techniques may also be extended to probe the orientation and alignment of the final J states by control of laser

Received: April 19, 2016
Revised: June 28, 2016
Published: June 29, 2016

DOI: 10.1021/acs.jpcc.6b03973
J. Phys. Chem. C 2016, 120, 16687−16698

polarization,[22,39−41] and therefore probe the stereodynamics and even the chirality of the collisional process.

However, none of the above scattering techniques gives a full account of the scattering process. Specifically, time-of-flight methods cannot detect the internal quantum state of the scattered molecules, while the laser-based methods have not usually been able to determine the full molecular vector velocities. In particular, correlations between translational and internal degrees of freedom in the scattered flux are likely to contain valuable insight into the details of gas−surface interactions, but have so far proven elusive. This Article presents results from a new surface-scattering technique, which detects both the internal state and the complete velocity components of the scattered molecules. The method combines state-selective 2 + 1 resonance-enhanced multiphoton ionization (REMPI) with 3D velocity-map imaging of the resulting ions, which allows for a full, 2π steradian reconstruction of the states of individual molecules leaving the interfacial region.

In the context of such a simple model for TD and IS scattering pathways, it is important to make some distinctions explicitly clear. Because of the longevity of the gas−interfacial interactions for TD events,[42−44] there is a physical expectation that both external (translational) and internal (rovibronic) quantum states will, or at least could, remain in a Boltzmann distribution at the surface temperature (T_S). This is not rigorously true, as the presence of explicit anisotropic or isotropic barriers to desorption can result in outgoing torques and forces in the exit channel that yield non-Boltzmann final rovibrational, velocity, and/or angular distributions for the desorbing molecular flux.[32] From a detailed balance perspective, the presence of such barriers would necessarily imply nonuniform efficiency for thermal accommodation (i.e., "sticking" or "trapping") of incident flux as a function of incident momenta and/or internal quantum states. Conversely, for a flux of desorbing molecules always in a Boltzmann distribution at the surface temperature, this implies near unity sticking coefficients for all incident quantum states, angles, and translational energies of gas molecules significantly sampled from a Boltzmann distribution at T_S.

The IS channel, on the other hand, is much less well-defined and dynamically constrained. At higher incident collision energies ($E_{inc} \gg kT_S$), where such IS channel deviations from perfect accommodation dynamics can and naturally do arise, there is no a priori expectation for a "simple" distribution in either external or internal states, which in general could be completely nonthermal. Furthermore, whereas rotationally hot molecules ($E_{rot} \gg kT_S$) in the outgoing flux have vanishingly low probabilities of arising from a long time, thermally accommodated molecule desorbing from the surface (i.e., TD events), there is no corresponding claim that even relatively prompt interactions (i.e., IS events) with the interface will not also yield some fraction of low rotational J states. Indeed, there is no assurance of any clean separation between TD and IS channel contributions, as first stressed by Hase and co-workers in molecular dynamics (MD) simulations of the rotational distributions.[45,46] However, what this Article nicely demonstrates is that, despite such a freedom of choice, the IS channel does appear to achieve a remarkable "hot but thermal" equilibration with respect to internal rovibrational quantum states, and indeed one that often closely matches the extent of translational excitation into the out-of-plane scattering directions.

The surfaces of particular interest for this experiment are self-assembled monolayers (SAMs) of alkanethiols on gold.[42,47−51] The surface presented by such a SAM to impinging molecules is made up of long alkyl chains, so that its scattering properties might be expected to begin to approximate those of a hydrocarbon liquid. Indeed, direct absorption studies of CO_2 scattering from perfluorinated polyether and fluorinated SAMs[27,29] exhibit remarkably quantitative agreement in scattering behavior between the true bulk liquid and such liquid-like mimetics. What makes this particularly powerful is that van der Waals forces between these chains cause them to spontaneously organize into highly organized crystal grains, with all head groups in one plane and facing in the same direction.[48,52] Thus, gas molecules arriving at the SAM surface interact predominantly with a known, chemically "tunable" surface moiety, which represents an enormous level of flexibility and control over the collision dynamics.

The organization of this Article is as follows. Section II describes the preparation and characterization of the SAM surfaces, as well as design of the velocity-map imaging apparatus with which to study them. In section III, we present quantum state- and vector velocity-resolved results and analysis for low-energy (0.7(1) kcal/mol) and high-energy (17(1) kcal/mol) scattering. Comparison of the inelastic dynamics elucidated by this work with other studies are discussed in section IV, with conclusions and directions for future/ongoing efforts summarized in section V.

II. EXPERIMENTAL SECTION

II.A. Sample Preparation and Characterization. The present studies involve scattering of thermal and hyperthermal HCl projectiles from well-ordered self-assembled monolayers, comprised of dodecane (C_{12}) aliphatic chains and made via standard SAM synthetic methods described in the literature.[17,48] Specifically, dodecane SAMs are grown on commercially purchased microscope slides precoated with polycrystalline gold, which are cleaned with piranha solution, rinsed with deionized water/ethanol, and immersed in a 1 mM dodecanethiol ($CH_3(CH_2)_{11}SH$)/ethanol solution for 12 h. As a result of (i) strong S−Au bond formation, (ii) rapid lateral surface diffusion, and (iii) weak van der Waals interactions, the dodecanethiol molecules self-organize into closely packed parallel structures of large islands, with an average 27° angle of the chain backbone to the surface normal.[48,52] AFM characterization[17,52] of such SAM surfaces indicates that these islands are typically 50−200 nm in diameter. Thus, over the macroscopic dimensions of the scattering beam (1 cm^2), the surfaces predominantly present methyl groups as a first layer "canopy" to the incident projectiles, but with a presumably uniform distribution over chain backbone azimuthal angles with respect to the surface normal.

The quality and uniformity of the resulting SAM interfaces are crucial to the quality and reproducibility of the experimental scattering data. Furthermore, this uniformity must be maintained over multiple hours to days in a high vacuum chamber, as a function of SAMs temperature and scattering conditions. This requires a relatively rapid and convenient optical probe of the SAMs surface, which may be achieved via reflection−absorption infrared spectroscopy[17,49] with a commercial FTIR spectrometer, specifically by characterization in the methyl and methylene stretch region near 2800−3000 cm^{-1}. A well-formed, crystalline SAM with translational symmetry and low entropy provides an identical local chemical

DOI: 10.1021/acs.jpcc.6b03973
J. Phys. Chem. C 2016, 120, 16687−16698

environment in each aliphatic chain, which results in four sharp RAIRS peaks corresponding to methyl and methylene CH stretching vibrations (see Figure 1), while poorly formed or

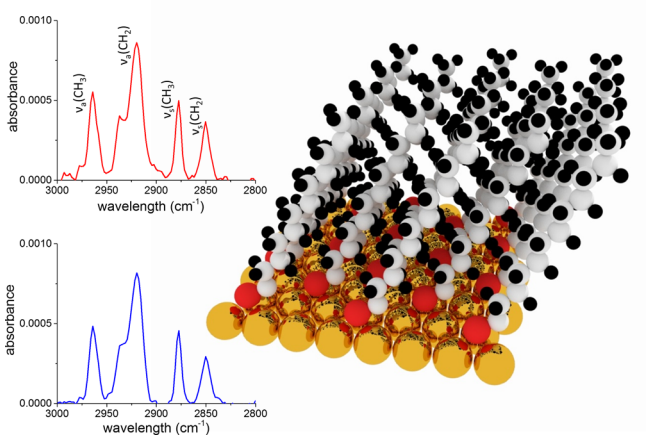

Figure 1. RAIRS spectra of dodecanethiol SAM on polycrystalline gold, (a) immediately after SAM formation and (b) after 8 h at 390 K in a vacuum, together with a cartoon depiction of the SAM (c). Both spectra exhibit the four characteristic peaks of a well-organized alkanethiol SAM.

damaged SAMs yield peaks that are inhomogeneously broadened and cannot be resolved. After RAIRS characterization, samples are placed in a vacuum chamber maintained at 5×10^{-9} Torr by one 1250 L/s and two 250 L/s turbo pumps. The sample mount also contains a cartridge heater, which can vary the sample temperature between 294 and 450 K. Repeated RAIRS measurements as a function of time indicate that dodecanethiol SAMs can withstand heating to 450 K under vacuum for up to 3 days without any spectroscopic evidence for deterioration. The sample is periodically removed from the vacuum chamber, characterized by RAIRS, and replaced as necessary.

II.B. Quantum-State Resolved DC-Sliced Velocity-Map Imaging. The above SAM surfaces are probed by grazing-angle HCl scattering with quantum-state and velocity-resolved detection. Aspects of the surface-scattering apparatus have been summarized elsewhere,[49,53] with modifications specific to the present studies described herein. In the present work, alkyl chain self-assembled monolayer surfaces are probed with HCl molecules at well-defined incident energies, and such energies may be produced and tuned via supersonic expansion. To tune the incident kinetic energy, 1% mixtures of HCl seeded in a systematic series of buffer gas diluent (H_2, He, Ar, and 30% He/70% Ne) are released into the vacuum through a 100 μm pinhole orifice pulsed valve[54] (200 μs duration, 10 Hz repetition rate). The supersonically cooled molecular beam passes through a 2 mm diameter skimmer 80 mm downstream from the pulsed valve, producing a narrow spread of transverse velocities (<3%) in the portion of the beam impinging on the sample. The valve and skimmer assembly are positioned such that the skimmed beam strikes the SAM surface at a 75° angle, and illuminates an elliptical region approximately 4 cm long and 1 cm wide. This grazing angle is convenient because it produces a large surface region illuminated by the molecular beam, allowing for detection of all departing velocities with a single ionization region. The beam typically achieves a velocity spread of $v/\Delta v = 10$ in the direction of travel, cooling >90% of the HCl molecules into the $J = 0$ ground rotational state.

The rovibrationally excited HCl(v,J) molecules resulting from elastic/inelastic scattering at the gas−SAMs interface are then gently ionized via one-color 2 + 1 REMPI.[55,56] The requisite light near 235 nm is produced by tripling the output of a tunable pulsed dye laser with LDS 698 dye, pumped by the 532 nm frequency doubled output of a pulsed Nd:YAG laser. The dye laser output is pre-expanded to a spot size of 15 mm before being focused into the chamber, to achieve a 50 μm waist in the ionization region. This region is positioned <1 mm above the center of the SAM surface, such that molecules with essentially all velocity components may be probed. Molecular ionization of the HCl proceeds via two steps: (i) 2-photon transition to a bound, intermediate state, followed by (ii) 1-photon transition to the ionization continuum. Thus, tuning the dye laser frequency allows for state-selective ionization of HCl(v,J) molecules with arbitrary velocities and a well specified angular momentum, typically $J = 0$−14. To minimize distortion of the ion cloud by Coulomb repulsion, the laser power is varied over a 10−120 μJ/pulse energy range to limit production to at most 30 ions per shot. At these ion densities, the repulsive effects due to Coulomb effects are negligible, indeed, notably smaller than the (approximately 18 m/s) distortion due to electron recoil.[49] This distortion, in turn, is comparable to the velocity spread of the incident beam for a 0.7(1) kcal/mol supersonic expansion in argon, and about 10 times smaller than the velocity spread for a 17(1) kcal/mol hydrogen expansion.

Our next task is to detect the state-selected velocities of these recently scattered HCl^+ and Cl^+ ions. The ionization region lies along the central stack of annular aluminum electrodes that form a velocity-map imaging system,[53,57−59] as depicted in Figure 2. The gold substrate of the SAM acts as a repeller electrode and is maintained at approximately 1400 V by means of electrical contacts at the edges of the sample slide. The first lens, second lens, and extractor electrodes are typically held at

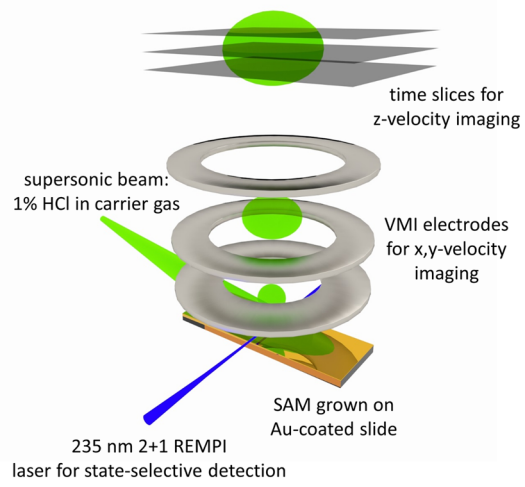

Figure 2. Velocity-map imaging apparatus for measurement of surface-scattered HCl. A pulsed supersonic beam of 1% HCl in 150 Torr buffer gas strikes a self-assembled monolayer surface grown on polycrystalline gold. A pulsed UV REMPI laser passes within 1 mm of the surface. Ionized molecules are extracted by a stack of three annular aluminum electrodes and impinge on a double-layer MCP, monitored by a CCD camera. The MCP voltages are pulsed so that only a thin slice of the ion cloud is imaged.

DOI: 10.1021/acs.jpcc.6b03973
J. Phys. Chem. C 2016, 120, 16687−16698

about 1100, 700, and 0 V, respectively. The electrode stack extracts ions upward from the ionization region, through a 50 cm vertical flight tube, and onto a position-sensitive two-stage microchannel plate detector. The electron signal from the MCP then strikes a phosphor screen and may be imaged by a CCD camera. With electrode voltages properly tuned to the velocity map configuration, ions with a given initial velocity component perpendicular to the sample surface normal (v_x, v_y) arrive at an easily predictable point on the detector, regardless of initial position. Also, ions with a larger initial upward velocity (v_z) reach the detector sooner, so ion arrival time provides a measurement of the final ion velocity component.[50] Therefore, the voltage across the MCP is maintained at 1300 V (~0 gain), and pulsed to 1700 V (~10^7 gain) for 80 ns during the arrival of the ion cloud. Under these conditions, ion clouds typically take ~700 ns to fully strike the MCP, which allows for 10 "slices" of the full cloud to be analyzed individually, with the resulting images scaled by the pulsed valve backing pressure, the square of the laser power (the ionization process is limited by the initial two-photon step), and the ionization efficiency of each J state.

The scale factors that relate v_x,v_y to detector position and v_z to detector arrival time are determined by imaging HCl molecules that have had time to equilibrate with the room-temperature (294 K) walls of the vacuum chamber. These molecular velocities should accurately reflect a thermal 3D Maxwell–Boltzmann distribution, and thus the (v_x, v_y) images are fit to 2D Gaussians to obtain the conversion factor from detected position to initial v_x,v_y of 10.7(1) (m/s)/pixel. Likewise, a fit of the total populations in each sliced image to a 1D Gaussian yields the conversion factor from time delay to v_z of 2.51(5) (m/s)/ns. The same thermal fits also permit the velocity origin on the MCP to be determined with high accuracy. Finally, comparison of total ion signals in each J state to a Boltzmann rotational distribution at room temperature allows a determination of the relative REMPI ionization efficiencies for each J state, which may differ by J state due to different rates of rotational predissociation of the intermediate REMPI state.[55,56] These calibration measurements are repeated several times per day during any other data collection to monitor any drift in the origin or scaling behavior of the imaging system.[49,53]

This technique offers several key advantages over conventional unsliced 2D velocity-map imaging. First, ionization techniques like VMI directly measure the molecule density in the ionization region, but do not offer full vector information on molecular flux leaving the surface. By way of contrast, the present experiment measures all three molecular velocity components. This allows rigorous density-to-flux conversions to be performed, facilitating a more quantitative comparison with mass-spectrometry-based surface-scattering experiments. Second, the ability to image in 3D velocity space permits such vector flux distributions to be obtained for species emerging into the full 2π steradians above the SAM surface, which therefore immediately provides complete differential scattering information both parallel and perpendicular to the scattering plane.

Of particular relevance to the current scattering geometry, the ability to resolve the velocity component along the surface normal allows for systematic elimination of strong ion signals arising from the incident beam. Simply stated, this naturally arises because HCl scattered from the surface generates ions with upward motion ($v_z > 0$), while ions from the incident beam are necessarily moving downward ($v_z < 0$). The value of such a separation is illustrated in Figure 3, where the quite

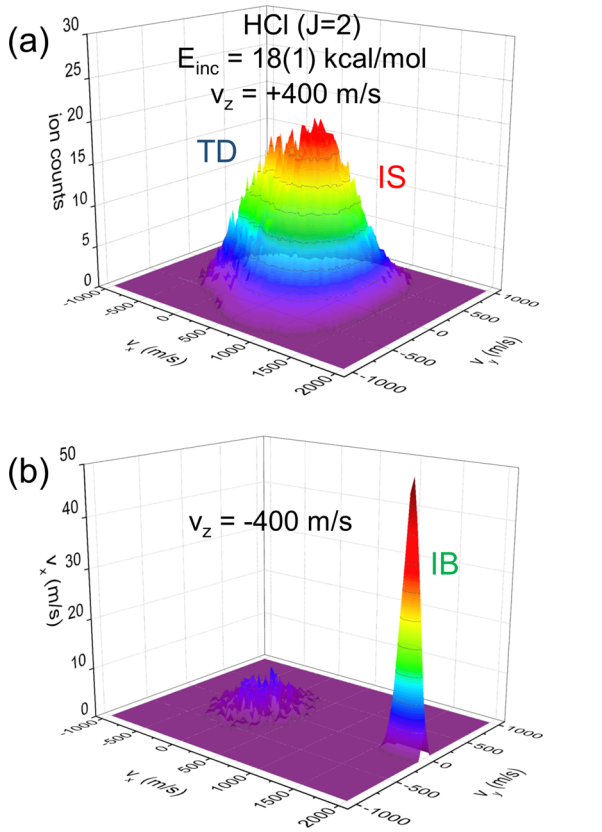

Figure 3. Representative v_z-slice imaging of molecules with initial upward (a) and downward (b) velocities revealing incident beam separation. Colors simply reflect increments along the vertical axes. The upward image contains trapping-desorption and impulsive scattering populations, while the downward image contains the incident beam. (See the 2D slices in Figure 6 for an even clearer separation of TD and IS contributions.)

strong incident beam signal appears in only one negative velocity slice ($v_z < 0$), while the ions from scattered molecules form broad structures across several positive velocity slices ($v_z > 0$). Also worth noting is that these 3D velocity space images immediately illustrate qualitative differences between the TD and IS scattering channels. As the TD contributions have lost all memory of the incident collision with the SAM surface, the corresponding TD signals are centered isotropically around $v_x = v_y = 0$, whereas the IS channel clearly peaks in the direction of the incident beam ($v_x > 0$). Similarly, the TD ion signals peak at small $v_z \approx 0$, whereas the IS scattered molecules are preferentially scattered upward with larger $v_z > 0$. Finally, and most importantly, the ability to achieve such clean separation of (i) incident and (ii) scattered signals permits rigorous normalization of all of the quantum state resolved scattered flux contributions.

III. RESULTS

III.A. Low Incident Energy Leads to Pure TD Scattering. We first consider the 3D angular/flux distributions of scattered HCl doped into a low-energy supersonic beam (E_{inc} = 0.7(1) kcal/mol), for which the incident HCl molecules might be expected to equilibrate with the SAM surface with

DOI: 10.1021/acs.jpcc.6b03973
J. Phys. Chem. C 2016, 120, 16687–16698

nearly 100% efficiency.[60] Because TD molecules by definition thermally accommodate prior to desorption, their behavior will depend on the surface temperature (T_S). Specifically, provided that the probability (α) of a molecule trapping long enough to lose memory is independent of incident energy, angle, or internal quantum state, then detailed balance considerations demand the desorbing densities to be a Maxwell−Boltzmann distribution at T_S. In general, however, this trapping or sticking probability will depend on incident energy, with the higher collision energy molecules more likely to scatter impulsively.[27,28,49] Thus, the more rigorous statement would be that if $\alpha \approx$ unity for the range of all thermal velocities typically sampled, the desorbing molecules will constitute a Maxwell−Boltzmann distribution at T_S, with velocity space densities given by a 3D Gaussian restricted to the upper half plane ($v_z > 0$).

Figure 4a,b presents a summary of results on desorbing velocity distributions for incident HCl seeded in argon (E_{inc} = 0.7(1) kcal/mol) and colliding with a dodecanethiol SAM at room temperature. The distributions are analyzed with 2D and 1D Gaussian fits for (v_x,v_y) (see Figure 4a) and $v_z > 0$ (see Figure 4b), respectively, which yield full width half maxima (fwhm) values in excellent agreement with the 294 K surface temperature. The quality of fit and agreement between the three $T_{x,y}$, T_z, and T_S values strongly support our basic model premise that scattering at such low incident energies is completely dominated by trapping-desorption and thermal equilibration. By way of additional confirmation, these measurements have also been performed as a function of T_S, with experimental temperatures arising from these velocity fits averaged over all HCl rotational states. As shown in Figure 4c, the results are in quantitative agreement with the actual surface temperature range of T_S = 294−400 K. Simply summarized, the present VMI capabilities establish that the TD scattering channel for HCl + SAMs surface is accurately described by a thermal velocity distribution at the surface temperature. By detailed balance considerations, this implies near unity trapping probabilities with respect to the incoming HCl for all speeds sampled typically for a sample at T_S.[60]

In addition to detailed velocity vector information on the translational degrees of freedom, the scattered HCl also desorbs in a rotational distribution probed by state-selective REMPI methods.[53,55,56] If sticking probabilities are unity for all HCl rotational states sampled, then detailed balance would predict that rotational distributions from pure TD events should be in equilibrium with the surface temperature. By way of quantitative support, Figure 5a displays sample Boltzmann plots of the outgoing rotational populations, integrated over all 3D velocities and for low (291(1) K) and high (364(1) K) surface temperatures. For both temperature extremes, the rotational populations are well fit to a single Boltzmann temperature (T_{rot}), which in turn is in excellent agreement with the experimental surface temperature (T_S). Again by way of confirmation, this procedure has been performed over a series of SAM surface temperatures, with the data plotted in Figure 5b. Within experimental error, the results are consistent with $T_{rot} \approx T_S$ over the full range of temperatures explored. The combination of Figures 4 and 5 provides direct evidence that low energy collisions of HCl from SAMs (i) stick with unit probability, independent of rotational quantum state and independent of velocity, for velocities populated in a Boltzmann distribution at T_S, and (ii) desorb with both rotational and translational degrees of freedom in close equilibrium with the

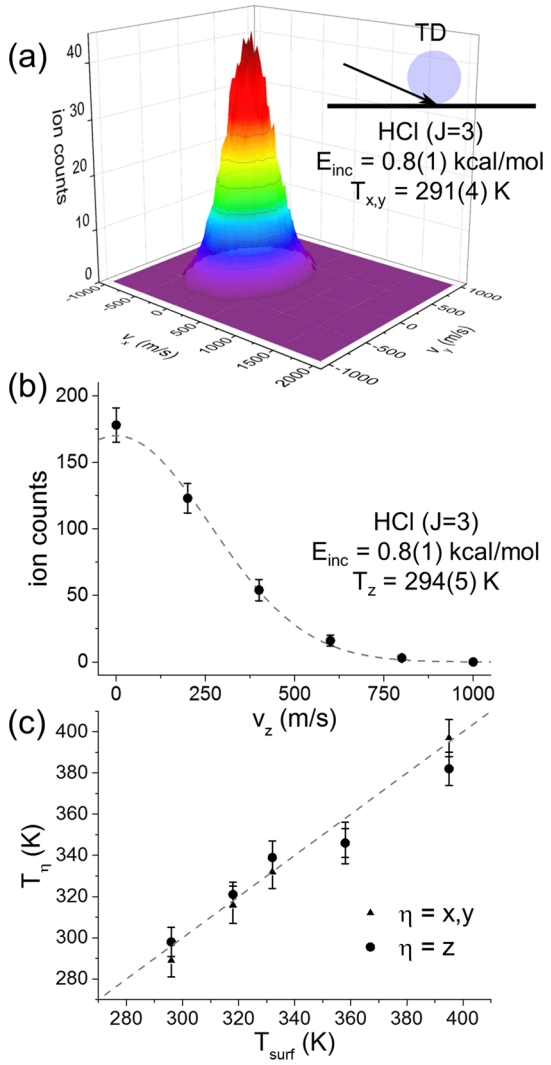

Figure 4. Representative v_z-integrated velocity map (a) and v_z profile (b) for HCl molecules that have been allowed to thermally equilibrate with the chamber walls. A two-dimensional symmetric Gaussian fit to the data in (a) and a one-dimensional Gaussian fit to (b) indicate temperatures of 291(4) and 294(5) K, respectively, in agreement with room temperature. Measured translational temperatures at various surface temperatures are summarized in (c). The translational temperature consistently matches the surface temperature.

surface temperature. We note that rapid equilibration between rotation/translation in the desorbing flux would be consistent with the small number of collisions required for thermalization of HCl under gas-phase conditions. Furthermore, we see no signals from vibrationally excited HCl (v = 1, J) at low collision energies with our current levels of experimental sensitivity. However, this is not surprising. If the vibrational degree of freedom from such a TD distribution were similarly equilibrated, the fraction of HCl (v = 1) molecules desorbing from a room-temperature SAM surface (~1 in 10^6) would be too small to detect with our current signal-to-noise and dynamic range.

III.B. TD and IS Scattering at High Incident Energy. With both of the translational/rotational populations well characterized under low collision energy conditions (i.e., $\alpha \approx 1$, pure TD scattering), we consider the more complex scattering dynamics at higher energy, which now must include the possibility of nonequilibrium, impulsive scattering (IS) events.

DOI: 10.1021/acs.jpcc.6b03973
J. Phys. Chem. C 2016, 120, 16687−16698

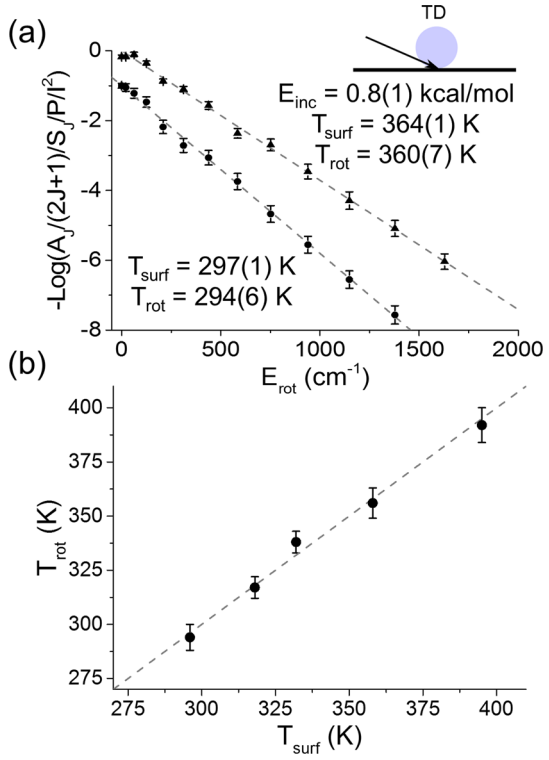

Figure 5. Boltzmann plot of rotational populations from a E_{inc} = 0.7(1) kcal/mol expansion at two different surface temperatures (a), and summary of HCl rotational temperatures at various surface temperatures (b). All measured HCl temperatures agree with the surface temperature to within the stated experimental uncertainty, consistent with detailed balance expectations with unity sticking coefficient for thermally populated internal and translational states.

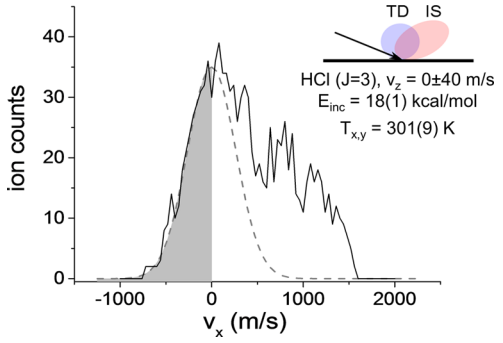

Figure 6. Example separation of an E_{inc} = 17(1) velocity map into TD and IS components. An 80 m/s wide slice along the x-axis produces the profile shown with the fitted region, $v_x < 0$, highlighted.

It is often stated that the impulsive scattering (IS) channel reflects interactions with the surface of "insufficient" duration to lose all memory of the incident collision.[27,37,61] This certainly captures one essential idea, but is experimentally ambiguous as to the meaning of insufficient. For example, if what we call the IS channel were fortuitously to yield an exact thermal distribution in equilibrium with the surface, such events would be indistinguishable from (and therefore absorbed into) the TD channel. An operationally more useful and, one might argue, the only meaningful description of the IS channel is that it reflects all deviations from pure TD behavior. We know from the above that pure TD x/y velocity components for HCl + dodecanethiol SAMs scattering are quantitatively predicted by a 2D (v_x, v_y) Gaussian distribution evaluated at T_S. Furthermore, it is physically reasonable to expect negligible contamination from the IS channel in the back half plane ($v_x < 0$) for scattering at such grazing 75° incidence. Thus, one can extract the nearly pure TD component by performing 2D Gaussian fits of the back half plane velocity events $[v_x < 0]$ to a Maxwell–Boltzmann distribution at some temperature T, as shown in Figure 6. Note that any assumptions can be independently tested by both (i) fit quality in the back half plane as well as (ii) agreement with the surface temperature (i.e., $T \approx T_S$). The impulsive scattering signals are then most simply obtained by difference between total signal and the 2D Gaussian fit for all v_x. In summary, the 2π velocity mapping imaging methods described in this work build on and extend some of the pioneering efforts in angle resolved rare gas atom scattering at metal surfaces[38] and offer an especially valuable, first-time capability for 3D separation of the TD and IS scattering flux contributions for molecular colliders as a function of internal rovibrational quantum state.

As the simple corollary, we can integrate over all final 3D velocities $[v_x, v_y]$ $[v_z > 0]$ and consider the TD and IS internal state populations of the scattered HCl molecules. It is worth noting that analysis of the rotational populations arising from the combined TD and IS scattering channels at high energies has frequently invoked fits to a two-temperature rotational distribution, with one temperature often fixed at the surface temperature (corresponding to the TD portion), and the other allowed to float (corresponding to a much hotter, albeit thermal IS rotational distribution).[27,28,32] The powerful advantage of such velocity-map methods is that they now allow unambiguous separation of each J-state resolved image into TD and IS components, without any prior assumptions imposed on the rotational distributions, and thus offer an opportunity for independent validation of such a two-temperature analysis. By way of example, Figure 7a and c displays sample Boltzmann plots for experimental rotational populations extracted separately from the least-squares fitted TD and IS components. Each yields a rotational distribution well-characterized by a single temperature out to $E_{rot} \approx 1600$ cm^{-1} (i.e., >7 kT_S). Least squares fits to the isolated TD populations return temperature values (T_{TD} = 293(7)K) in excellent agreement with the measured SAMs surface and indeed as expected for fully thermally equilibrated collisional interactions. Even more notably, the IS rotational states also appear Boltzmann in character, with a hyperthermal albeit temperature-like distribution quantitatively consistent with those obtained from simultaneous two-temperature fits to the total quantum state populations. It warrants mention that such simplicity in the IS rotational distributions neither implies nor requires similar simplicity in the corresponding translational flux distributions, which in fact are highly anisotropic and strongly forward scattered in the near specular direction.

Although we have seen evidence for this in a number of previous spectroscopic studies of gas–liquid scattering dynamics,[28,29,42,49,53] it is worth emphasizing that this is a very surprising result. Indeed, it is simply not obvious why the IS component of the HCl rotational populations should conform so well to some hyperthermal Boltzmann distribution, with temperatures (T_{IS} = 930(20) K) much higher than T_S. As one of many alternative scenarios, for example, one might have expected distributions more reminiscent of rotational rainbow effects evident in gas-single crystal scattering studies.[22,35,38,62,63] Of course, it could simply be that the greater roughness of the

DOI: 10.1021/acs.jpcc.6b03973
J. Phys. Chem. C 2016, 120, 16687–16698

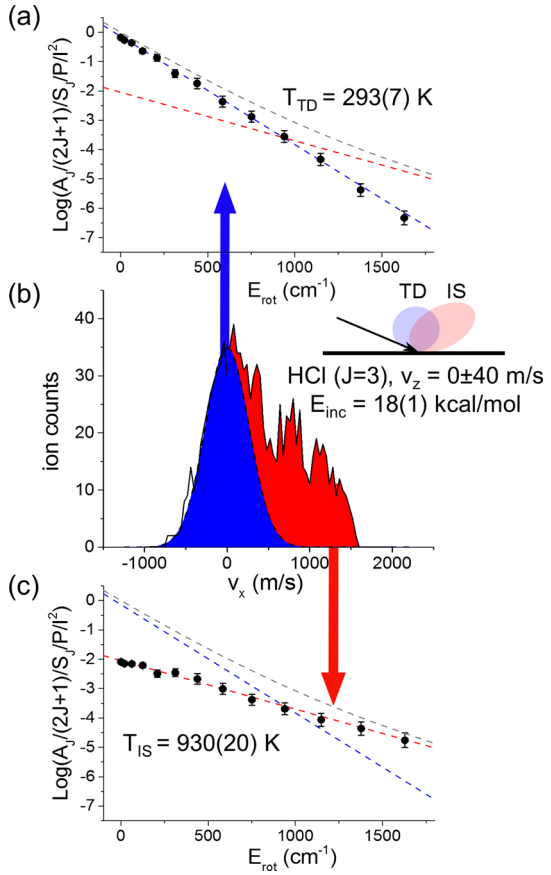

Figure 7. Example separation of an ion image into TD (blue) and IS (red) populations (b), together with single-temperature fits to the rotational distributions of the individual TD (a) and IS (b) populations. Each population is well described by a single rotational temperature, with the TD population matching the surface temperature and the IS population much hotter.

surface due to capillary wave excitation[64−66] blurs any such rainbow effects. Yet if so, this does not explain why the HCl rotational distributions would appear so thermal out to such high kT_S values of internal energy (see Figure 7c). One simple physical picture could be that the dynamics arise from localized heating of the SAM surface by high-energy impact of the gas molecule impact, producing a local "hot spot" with which the molecule might be rotationally heated on the accelerated time scale of an IS event.[67] We will return to this idea in the Discussion section. In any event, the ability of VMI methods to independently extract the TD versus IS components by backscattered final velocities provides unambiguous support for the existence of hyperthermal albeit Boltzmann rotational distributions in the IS channel, which in turn must signal the presence of simplifying dynamical constraints in the gas-SAMs rotational excitation process. Clearly higher level theoretical investigation will be necessary to explore these issues further, toward which we hope these quantitative results on such a simple model system may offer sufficient stimulation.

As a final comment for the Results section, the vibrational spacing for HCl is $\hbar\omega_0 \approx 8.5$ kcal/mol, and thus collision conditions ($E_{inc} = 17(1)$ kcal/mol) are sufficient to populate up to HCl($v = 2$). Despite such energetic accessibility, we do not detect any vibrationally excited HCl at these high collision energies, with HCl($v = 1$) populations down from HCl($v = 0$) by at least 1000-fold and below our current limit of our experimental sensitivity. There is, however, very good reason to expect this process to be vibrationally adiabatic. Specifically, the period for HCl vibration ($T \approx 12$ fs) is 2 orders of magnitude shorter and therefore very poorly matched with the picosecond time scale[42−44] of any impulsive interaction with the surface, rendering vibrational excitation extremely inefficient. Thus, as was the case for low incident energy, neither appreciable vibrational excitation nor relaxation is anticipated and is indeed not observed. The vibrational degree of freedom acts like a spectator in the dynamics, which is entirely consistent with the previous vibrational excitation inefficiency[27,28] noted for even 4-fold lower frequency bend excitation in CO_2 ($\hbar\omega_0 \approx 1.9$ kcal/mol) via hyperthermal collisions at the gas−liquid interface.

IV. DISCUSSION

IV.A. Sticking Coefficients. One crucial piece of information available from our analysis of the signals is the fraction of hyperthermal collisions that proceed by TD vs IS (or, equivalently stated, the non-TD) channel. Note that these VMI signals are collected with near unity quantum yield in full 2π steradians, which therefore includes both in-plane and out-of-plane scattering contributions into any final solid angle. This represents a crucial advantage over previous mass spectrometric studies, which typically probe in the scattering plane (with notable heroic exceptions),[6,7,15,16,21,26,66,68] often in a fixed, near specular direction and always restricted to some angular range outside of the incident beam. Indeed, for molecular projectiles amenable to REMPI detection, this highly multiplexed, high throughput VMI capability also significantly outstrips capabilities from previous quantum state resolved studies in our group based on high-resolution direct absorption[27−32] and laser-induced fluorescence[32] spectroscopic methods. Of particular importance, the ability to isolate, probe, and quantitatively compare incoming versus scattered signals by DC slicing and integrating over $v_z < 0$ or $v_z > 0$ acceptance windows permits one to rigorously measure the fraction of incident HCl flux that reappears in the scattering distributions under the steady-state conditions of $a \approx 200$ μs long gas pulse. For the present study of dodecanethiol SAMs, this recovery fraction is found to be >99.5(0.7)%, that is, unity within experimental uncertainties. For future reference, we note that this is definitely not always the case, and can be substantially less than unity for HCl scattering on "high pK_a" amine terminated SAMs or H/D proton exchange on "low pK_a" COOH terminated SAMs, respectively.

Furthermore, the current velocity-map imaging capabilities also offer two independent ways to compute the sticking coefficient for HCl on hydrocarbon SAMs at a particular incident energy. Specifically, α can be obtained via amplitude ratios either in (i) a "two-temperature" (i.e., TD + IS) fit to rotational populations and then integrating over all velocities (labeled "rotational populations" in Figure 8a,b), or by (ii) deconstruction of each image into TD and IS portions (by least-squares fitting TD fractions to the back half plane velocities) and then summing over all final J states in each channel (labeled "ion images"). Figure 8a and b displays the resulting sticking coefficients obtained for HCl expansions as a function of incident beam energy (E_{inc}) by varying the gas diluent [H_2 (17(1) kcal/mol), He (13(1) kcal/mol), Ne-70 (5(1) kcal/mol)] for a constant HCl mole fraction. As expected, molecular projectiles with greater incident energies systematically exhibit a smaller propensity for trapping−

DOI: 10.1021/acs.jpcc.6b03973
J. Phys. Chem. C 2016, 120, 16687−16698

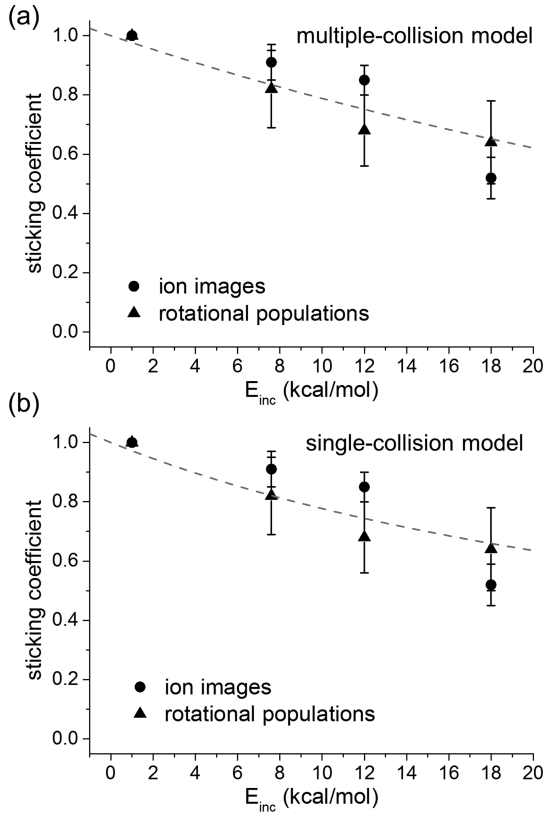

Figure 8. Sticking coefficients obtained directly from separation of TD and IS components in ion images and from two-temperature fits, at various HCl incident energies, and analyzed according to (a) single collision and (b) multiple collision models (see text for details). The sticking coefficient decreases with incident energy, with a $1/e$ energy of 34(4) kcal/mol.

desorption events, and thus bounce promptly off the surface to yield lower sticking coefficients.

We offer two very simple physical models with which to characterize this drop in sticking coefficient (α) with increasing incident energy. First, we consider a "single collision" model, which proposes that the requisite momentum loss to accommodate on the surface occurs in a single interaction, but treats this interaction in a statistical fashion. A molecule with incident momentum p_z component perpendicular to the surface normal (and corresponding "normal" energy $E_n = p_z^2/2m$) encounters an attractive well of depth E_{well}, and thus must dispose of a total energy $E_n^{tot} = E_n + E_{well}$ upon striking the SAM surface. If we assume arbitrarily that this energy randomizes uniformly between $[0, E_n^{tot}]$ in this single collision and therefore escapes only if the resulting energy is greater than the well depth, then the surface trapping probability can be readily shown to be $\alpha = E_{well}/E_n + E_{well}$. Analysis of the incident energy-dependent sticking coefficients to this single collision model is presented in Figure 8a, where the dotted line represents a least-squares fit to the data and exhibits reasonable agreement with the experimentally observed trends. Although quantitative agreement from such a heuristic model is not to be expected, it is worth noting that the inferred value for E_{well} = 2.3(1) kcal/mol is within a factor of 2 of our ab initio CCSD(T)/vnZ-f12 predictions of the 1D well depth for HCl approaching a methyl-terminated hydrocarbon ($E_{CCSD(T)} \approx 1.2$ kcal/mol).

In a slightly more sophisticated "multiple collision" model, we assume that the incident molecule undergoes many sequential collisional interactions with the surface, each removing an energy (ΔE) from the projectile and each providing a new opportunity for ejection. The probability per interaction resulting in ejection is p, with conversely a $(1 - p)$ probability per interaction for remaining on the surface. The TD channel therefore corresponds to loss of all incident projectile energy without being ejected. Stated alternatively, to trap quasi-irreversibly on the surface, a molecule must survive $n \approx E/\Delta E$ collisions of probability $(1 - p)$, which therefore happens with a net probability:

$$P_{TD} = \alpha = (1 - p)^{E/\Delta E} = (1 - (pE/\Delta E/n))^n \approx \exp(-pE/\Delta E)$$

where the final expression in terms of an exponential is exact in the limit of $n = E/\Delta E \gg 1$. This model makes two simple predictions: (i) the sticking coefficient α decays exponentially with the incident energy and (ii) the characteristic decay rate $(p/\Delta E)$ reflects the probability of ejection per unit energy loss in a single collision. If we apply this model to the experimental data on α for hyperthermal collisions of HCl with a C_{12} SAM surface (see Figure 8b), we also find a similarly respectable fit, with $p/\Delta E$ = 0.029(5) mol/kcal and therefore predicting a characteristic collision energy of 34(4) kcal/mol for a $1/e$ loss in α. Although the current seeded pulsed valve experiments are limited to a relatively modest range of collision energies (E_{inc} < 20 kcal/mol), it would be interesting to systematically test predictions of such models with the much higher collision energies accessible, for example, from laser photolysis methods of McKendrick[26,69,70] or CO_2 laser detonation sources of Minton and co-workers.[6−8,68]

IV.B. Energy Redistribution in the IS Channel. In addition to vector characterization of the scattered velocity distributions, the present quantum state resolved VMI methods also make it possible to investigate potential correlation for scalar energy transfer between external (i.e., translational) and internal (i.e., rovibrational) excitation of the HCl. Data on the fractional energy transfer into rotation and translation are summarized in Figure 9, which indicate a roughly linear scaling with incident energy and therefore slopes that report on the efficiency for transfer into a particular degree of freedom. The outgoing HCl clearly retains nearly one-half (χ_{trans} = 48(7)%)

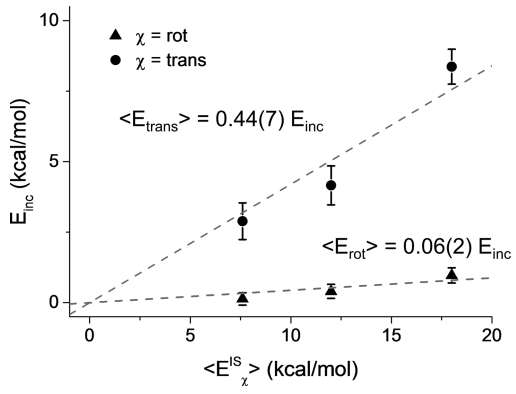

Figure 9. Summary of collisional energy redistribution in the IS channel for various incident energies. The departing molecules have on average 44(7)% of their incident energy in the translational degree of freedom, and 6(2)% in rotation.

DOI: 10.1021/acs.jpcc.6b03973
J. Phys. Chem. C 2016, 120, 16687−16698

of the incident energy in translation, with only a small fraction (χ_{rot} = 6(2)%) being converted to rotational excitation and the energy difference (χ_{loss} = 46(8)%) lost to collisional heating of the SAM surface. This predominance of translational versus rotational pathways for energy transfer is in stark contrast with comparable studies of CO_2 scattering from hydrocarbon liquids such as squalane,[27−29,31] for which the incident energy of the projectile was found to be more comparably converted into rotational (χ_{rot} = 34(3)%) and translational (χ_{trans} = 26(3)%) degrees of freedom, with a similar remainder (χ_{loss} = 40(5)%) of the incident energy deposited into the liquid interface.

There may be several mechanisms contributing to this qualitative difference in rotational/translational energy branching behavior, each based on the significant differences in rotational constants for the two projectiles, $B_{HCl} \approx 10.5$ cm^{-1}, $B_{CO2} \approx 0.4$ cm^{-1}. Let us suppose the projectile scatters by means of a single brief interaction with the surface, and the same impulse is applied to each molecule. The incident HCl and CO_2 molecular beams are cooled mostly down into the J = 0 rotational state, which, if we can simply neglect steering of the molecule by long-range attractive forces,[43,71] would imply an isotropic orientation of the first interaction. CO_2 dynamics will therefore be dominated by O atom collisions striking the surface, producing a classical lever arm on the order of the CO bond length (r_{CO} = 1.16 Å).[72] Conversely, HCl has its center of mass very close to the Cl atom, with surface collisions of the much larger Cl target atom resulting in a $m_H/m_{HCl} \approx 0.028\times$ smaller moment arm. Consequently, even for equal impulses applied to each molecule, CO_2 experiences a larger average torque than HCl, thus producing more efficient transfer of incident translational energy into rotation.

Furthermore, there can also be subsequent collisional dynamics of HCl and CO_2 molecules with similar rotational excitation from a first collisional interaction with the surface. Because HCl has the larger rotational constant ($B_{HCl} \approx 10.5$ cm^{-1}, $B_{CO2} \approx 0.4$ cm^{-1}), for a given rotational energy it will be classically rotating ∼5.1 times faster than CO_2. Thus, for typical 1−2 ps collision time scales at the gas−liquid interface,[42−44] the proton end of the HCl will have a substantially greater probability of rotating and striking the surface a second time, therefore receiving a collisional torque in opposition to the initial rotational excitation. The HCl versus CO_2 populations thus (i) start with lower rotational excitation on average, and (ii) have additional opportunities to reduce this energy further through secondary collisions with the gas liquid interface. A direct test of these simple models would be comparison of fractional energy deposition for HCl and DCl projectiles, for which the rotational constants differ by nearly 2-fold but the intermolecular potential for collisional interaction with the liquid surface is essentially identical.

C. 3D TD and IS Flux Distributions. As a final point of discussion, the complete 3D velocity information provided by DC-sliced VMI methods allows for direct determination of the outgoing molecular flux as a function of solid angle. The desired flux may be computed as follows. The velocity maps provide a direct measurement of $\rho(v_x,v_y,v_z)$, the density in velocity space of molecules leaving the surface with a particular 3D velocity $\mathbf{v} = (v_x,v_y,v_z)$ and in a volume element $dv_x\, dv_y\, dv_z$. The vector flux of molecules is then $v\rho(v_x,v_y,v_z)$ or $v\rho(v,\theta,\phi)$ when equivalently transformed into spherical coordinates. Sufficiently far from the scattering center, the total flux into a given solid angle may then be obtained from an integral over all scalar speeds:

$$F(\theta, \phi) = \int_0^\infty v\rho(v, \theta, \phi)v^2\, dv\sin(\theta)\, d\theta\, d\phi$$

which can be evaluated numerically.

Examples of the resulting flux distributions for low and high incident energies are presented in Figure 10 and reveal several

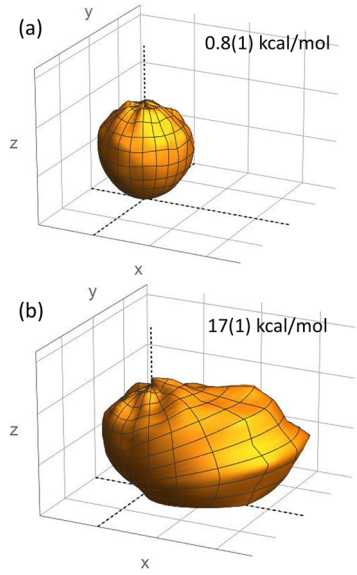

Figure 10. Relative molecular flux leaving the surface, integrated over all speeds and J-states at each solid angle, for (a) pure-TD events (surface probed by HCl seeded in Ar) and (b) TD + IS events (surface probed by HCl seeded in H_2). Flux distributions for individual J-states differ in details but look relatively similar.

interesting features. First, in the absence of any exit channel barriers to desorption, detailed balance considerations require that the flux distribution for all HCl molecules, which have equilibrated with the surface (i.e., the TD scattering component), should reflect a pure cos(θ) distribution. Figure 10a shows a plot of the experimentally measured outgoing flux distribution for HCl seeded in Ar (E_{inc} = 0.7(1) kcal/mol), which, from the above translational and rotational distributions as a function of T_S, has been demonstrated to exhibit essentially pure-TD scattering behavior at all liquid temperatures. In agreement with this expectation, the measured flux distribution clearly comprises a sphere that touches the velocity origin and extends in the +z direction, providing direct confirmation of a cos(θ) distribution characteristic of barrierless TD collisional events.

The corresponding angular flux distributions for high energy (17(1) kcal/mol) scattering events are shown in Figure 10b. In this case, the distribution is again quite spherical for $v_x < 0$, as would indeed be expected for molecules solely appearing in the back half plane ($v_x < 0$) from TD events. On the other hand, the distribution is now strongly asymmetrical, with a high propensity for lobular scattering into the forward half plane and at a slightly subspecular angle of 60(10)°. This result agrees quite nicely with previous results inferred from Dopplerimetry-based measurements of CO_2 flux departing from perfluorinated liquid surfaces, which was consistent with symmetrical distributions for scattering at normal incidence, and progressively more peaked, lobular distributions with increasingly grazing angle of incidence.[29,31] However, because such high-resolution Dopplerimetry measurements inform only on the

DOI: 10.1021/acs.jpcc.6b03973
J. Phys. Chem. C 2016, 120, 16687−16698

velocity component parallel to the probe laser direction, it is worth noting that such studies require sampling of multiple scattering geometries and are often completely insensitive to the velocity component normal to the liquid interface. By way of contrast, the present velocity map imaging capabilities constitute by far the more powerful and general approach, which provide information on all three translational degrees of freedom, allow for a completely rigorous density-to-flux transformation, as well as permit straightforward separation of the resulting quantum state resolved fluxes into TD and IS components.

V. SUMMARY AND CONCLUSION

Resonance-enhanced multiphoton ionization coupled to DC-sliced velocity-map imaging enables measurement of surface scattered molecular distributions with unprecedented detail. Measurement of the full scattered velocity distribution provides methods to separate the incident beam, trapping-desorption channel, and impulsive scattering channel. Direct separation of TD and IS offers a new avenue to precisely measure sticking coefficients, and the behavior of these sticking coefficients with varying energy gives insight into the detailed dynamics of energy transfer from incident molecules into the SAM surface. Correlated velocity and internal quantum state measurements provide a unique confirmation of the accuracy of two-temperature fits to scattered rotational distributions. These same correlated measurements also allow measurement of the rapid redistribution of energy among different degrees of freedom during impulsive scattering events, with significant energy being transferred to the surface or remaining in translation and only modest rotational excitation, in stark contrast with similar measurement for CO_2-liquid scattering. Full velocity information also allows for rigorous conversion between molecule density and flux for either the full outgoing distribution or the TD and IS channels separately, and thus for straightforward analysis of IS scattering-angle effects. The measured angular distributions for the molecular flux have been shown to match the anticipated $\cos(\theta)$ distribution for TD dominated events at either low energy or scattering into the back half plane ($v_x < 0$), but with the IS component exhibiting a strongly anisotropic, forward-scattered lobe peaking at near but slightly subspecular angles.

The breadth and flexibility of this technique offer considerable opportunities for further detailed exploration into collision dynamics at gas−liquid and gas−SAM interfaces. For example, sticking-coefficient measurements can provide information about how the interfacial surface characteristics change as a function of SAM alkyl chain length or headgroup. For example, longer saturated hydrocarbon chains might be expected to produce softer surfaces, with a dependence on the odd versus even chain lengths due to different orientations of the methyl head groups.[48,52,73] Conversely, hydrogen bonding between hydroxylated SAMs head groups may lead to a more strongly coordinated surface, with a corresponding increase in interfacial stiffness of the SAM canopy.[48,52] Scattering with DCl/HCl beams can be used to probe for proton exchange at various chemically modified (e.g., OH-, NH_2-, or COOH-terminated) SAM surfaces.[24,25,36] Stereodynamics at the surface may also be investigated by means of polarized REMPI laser excitation, which in turn allows for investigation of the final M_J distributions and thus torques experienced by molecules leaving the surface.[39−41] Critical to all such investigations would be the unprecedented access offered by VMI methods to correlated 3D translational and internal quantum state distributions in the scattered molecular flux.

AUTHOR INFORMATION

Corresponding Author

*E-mail: djn@jila.colorado.edu.

Notes

The authors declare no competing financial interest.

ACKNOWLEDGMENTS

This work has been supported by the Air Force Office of Scientific Research (FA9550-12-1-0139), with additional funds for vacuum equipment and lasers provided by the National Science Foundation (CHE1266416, PHYS1125844).

REFERENCES

(1) Andersson, P. U.; Nagard, M. B.; Pettersson, J. B. C. Molecular Beam Studies of HCl Interactions with Pure and HCl-Covered Ice Surfaces. *J. Phys. Chem. B* **2000**, *104*, 1596−1601.

(2) Batista, E. R.; Ayotte, P.; Bilic, A.; Kay, B. D.; Jonsson, H. What Determines the Sticking Probability of Water Molecules on Ice? *Phys. Rev. Lett.* **2005**, *95*, 223201.

(3) Chang, Q.; Cuppen, H. M.; Herbst, E. Gas-Grain Chemistry in Cold Interstellar Cloud Cores with a Microscopic Monte Carlo Approach to Surface Chemistry. *Astron. Astrophys.* **2007**, *469*, 973−983.

(4) Herbst, E. Chemistry in the Interstellar-Medium. *Annu. Rev. Phys. Chem.* **1995**, *46*, 27−53.

(5) Willacy, K.; Langer, W. D. The Importance of Photoprocessing in Protoplanetary Disks. *Astrophys. J.* **2000**, *544*, 903−920.

(6) Shpilman, Z.; Gouzman, I.; Grossman, E.; Shen, L. H.; Minton, T. K.; Paci, J. T.; Schatz, G. C.; Akhvlediani, R.; Hoffmann, A. Oxidation and Etching of Cvd Diamond by Thermal and Hyperthermal Atomic Oxygen. *J. Phys. Chem. C* **2010**, *114*, 18996−19003.

(7) Minton, T. K.; Wright, M. E.; Tomczak, S. J.; Marquez, S. A.; Shen, L.; Brunsvold, A. L.; Cooper, R.; Zhang, J.; Vij, V.; Guenthner, A. J. Atomic Oxygen Effects on Poss Polyimides in Low Earth Orbit. *ACS Appl. Mater. Interfaces* **2012**, *4*, 492−502.

(8) Paci, J. T.; Minton, T. K.; Schatz, G. C. Hyperthermal Oxidation of Graphite and Diamond. *Acc. Chem. Res.* **2012**, *45*, 1973−1981.

(9) D'Andrea, T. M.; Zhang, X.; Jochnowitz, E. B.; Lindeman, T. G.; Simpson, C. J. S. M.; David, D. E.; Curtiss, T. J.; Morris, J. R.; Ellison, G. B. Oxidation of Organic Films by Beams of Hydroxyl Radicals. *J. Phys. Chem. B* **2008**, *112*, 535−544.

(10) Cremer, P. S.; Su, X. C.; Shen, Y. R.; Somorjai, G. A. Ethylene Hydrogenation on Pt(111) Monitored in Situ at High Pressures Using Sum Frequency Generation. *J. Am. Chem. Soc.* **1996**, *118*, 2942−2949.

(11) Xu, C.; Yang, W.; Guo, Q.; Dai, D.; Minton, T. K.; Yang, X. Photoinduced Decomposition of Formaldehyde on a Tio2(110) Surface, Assisted by Bridge-Bonded Oxygen Atoms. *J. Phys. Chem. Lett.* **2013**, *4*, 2668−2673.

(12) Cheng, C. C.; Lucas, S. R.; Gutleben, H.; Choyke, W. J.; Yates, J. T. Atomic Hydrogen-Driven Halaogen Extraction from Si(100) - Eley-Rideal Surface Kinetics. *J. Am. Chem. Soc.* **1992**, *114*, 1249−1252.

(13) Jackson, B.; Persson, M.; Kay, B. D. Quantum-Mechanical Study of H(G)+Cl-Au(111) - Eley-Rideal Mechanism. *J. Chem. Phys.* **1994**, *100*, 7687−7695.

(14) Fan, S. M.; Jacob, D. J. Surface Ozone Depletion in Arctic Spring Sustained by Bromine Reactions on Aerosols. *Nature* **1992**, *359*, 522−524.

(15) Nathanson, G. M. Molecular Beam Studies of Gas-Liquid Interfaces. *Annu. Rev. Phys. Chem.* **2004**, *55*, 231−255.

(16) Saecker, M. E.; Govoni, S. T.; Kowalski, D. V.; King, M. E.; Nathanson, G. M. Molecular-Beam Scattering from Liquid Surfaces. *Science* **1991**, *252*, 1421−1424.

(17) Laibinis, P. E.; Whitesides, G. M.; Allara, D. L.; Tao, Y. T.; Parikh, A. N.; Nuzzo, R. G. Comparison of the Structures and Wetting

DOI: 10.1021/acs.jpcc.6b03973
J. Phys. Chem. C 2016, 120, 16687−16698

Properties of Self-Assembled Monolayers of Normal Alkanethiols on the Coinage Metal Surfaces, Cu, Ag, Au. *J. Am. Chem. Soc.* **1991**, *113*, 7152−7167.
(18) Osawa, M. Dynamic Processes in Electrochemical Reactions Studied by Surface-Enhanced Infrared Absorption Spectroscopy (Seiras). *Bull. Chem. Soc. Jpn.* **1997**, *70*, 2861−2880.
(19) Shen, Y. R. Surface Properties Probed by 2nd-Harmonic and Sum-Frequency Generation. *Nature* **1989**, *337*, 519−525.
(20) Bredenbeck, J.; Ghosh, A.; Nienhuys, H.-K.; Bonn, M. Interface-Specific Ultrafast Two-Dimensional Vibrational Spectroscopy. *Acc. Chem. Res.* **2009**, *42*, 1332−1342.
(21) Nathanson, G. M.; Davidovits, P.; Worsnop, D. R.; Kolb, C. E. Dynamics and Kinetics at the Gas-Liquid Interface. *J. Phys. Chem.* **1996**, *100*, 13007−13020.
(22) Kubiak, G. D.; Hurst, J. E.; Rennagel, H. G.; McClelland, G. M.; Zare, R. N. Direct Inelastic-Scattering of Nitric Oxide from Clean Ag(111) - Rotational and Fin-Structure Distributions. *J. Chem. Phys.* **1983**, *79*, 5163−5178.
(23) Rahinov, I.; Cooper, R.; Yuan, C.; Yang, X. M.; Auerbach, D. J.; Wodtke, A. M. Efficient Vibrational and Translational Excitations of a Solid Metal Surface: State-to-State Time-of-Flight Measurements of HCl(V = 2,J = 1) Scattering from Au(111). *J. Chem. Phys.* **2008**, *129*, 16.
(24) Ringeisen, B. R.; Muenter, A. H.; Nathanson, G. M. Collisions of HCl, Dcl, and Hbr with Liquid Glycerol: Gas Uptake, D -> H Exchange, and Solution Thermodynamics. *J. Phys. Chem. B* **2002**, *106*, 4988−4998.
(25) Ringeisen, B. R.; Muenter, A. H.; Nathanson, G. M. Collisions of Dcl with Liquid Glycerol: Evidence for Rapid, near-Interfacial D -> H Exchange and Desorption. *J. Phys. Chem. B* **2002**, *106*, 4999−5010.
(26) Tesa-Serrate, M. A.; Marshall, B. C.; Smoll, E. J., Jr.; Purcell, S. M.; Costen, M. L.; Slattery, J. M.; Minton, T. K.; McKendrick, K. G. Ionic Liquid-Vacuum Interfaces Probed by Reactive Atom Scattering: Influence of Alkyl Chain Length and Anion Volume. *J. Phys. Chem. C* **2015**, *119*, 5491−5505.
(27) Perkins, B. G.; Haber, T.; Nesbitt, D. J. Quantum State-Resolved Energy Transfer Dynamics at Gas-Liquid Interfaces: Ir Laser Studies of CO2 Scattering from Perfluorinated Liquids. *J. Phys. Chem. B* **2005**, *109*, 16396−16405.
(28) Perkins, B. G.; Nesbitt, D. J. Quantum-State-Resolved CO2 Scattering Dynamics at the Gas-Liquid Interface: Incident Collision Energy and Liquid Dependence. *J. Phys. Chem. B* **2006**, *110*, 17126−17137.
(29) Perkins, B. G.; Nesbitt, D. J. Toward Three-Dimensional Quantum State-Resolved Collision Dynamics at the Gas-Liquid Interface: Theoretical Investigation of Incident Angle. *J. Phys. Chem. A* **2009**, *113*, 4613−4625.
(30) Zolot, A. M.; Harper, W. W.; Perkins, B. G.; Dagdigian, P. J.; Nesbitt, D. J. Quantum-State Resolved Reaction Dynamics at the Gas-Liquid Interface: Direct Absorption Detection of HF(V,J) Product from F(P-2) Plus Squalane. *J. Chem. Phys.* **2006**, *125*, 21101.
(31) Perkins, B. G.; Nesbitt, D. J. High Resolution Dopplerimetry of Correlated and Quantum State-Resolved CO2 Scattering Dynamics at the Gas-Liquid Interface. *Phys. Chem. Chem. Phys.* **2010**, *12*, 14294−14308.
(32) Ziemkiewicz, M. P.; Roscioli, J. R.; Nesbitt, D. J. State-to-State Dynamics at the Gas-Liquid Metal Interface: Rotationally and Electronically Inelastic Scattering of No (2)Pi(1/2)(0.5) from Molten Gallium. *J. Chem. Phys.* **2011**, *134*, 234703.
(33) Huang, Y. H.; Rettner, C. T.; Auerbach, D. J.; Wodtke, A. M. Vibrational Promotion of Electron Transfer. *Science* **2000**, *290*, 111−114.
(34) Kleyn, A. W.; Luntz, A. C.; Auerbach, D. J. Rotational Energy Transfer in Direct Inelastic Surface Scattering - No on Ag(111). *Phys. Rev. Lett.* **1981**, *47*, 1169−1172.
(35) Rettner, C. T.; Fabre, F.; Kimman, J.; Auerbach, D. J. Observation of Direct Vibrational-Excitation in Gas-Surface Collisions - No on Ag(111). *Phys. Rev. Lett.* **1985**, *55*, 1904−1907.
(36) Lohr, J. R.; Day, B. S.; Morris, J. R. Scattering, Accommodation, and Trapping of HCl in Collisions with a Hydroxylated Self-Assembled Monolayer. *J. Phys. Chem. B* **2005**, *109*, 15469−15475.
(37) Hurst, J. E.; Becker, C. A.; Cowin, J. P.; Janda, K. C.; Wharton, L.; Auerbach, D. J. Observation of Direct Inelastic-Scattering in the Presence of Trapping-Desorption Scattering - Xe on Pt(111). *Phys. Rev. Lett.* **1979**, *43*, 1175−1177.
(38) Hurst, J. E.; Wharton, L.; Janda, K. C.; Auerbach, D. J. Direct Inelastic-Scattering Ar from Pt(111). *J. Chem. Phys.* **1983**, *78*, 1559−1581.
(39) Kummel, A. C.; Sitz, G. O.; Zare, R. N. Determination of Orientation of the Ground State Using Two-Photon Nonresonant Excitation. *J. Chem. Phys.* **1988**, *88*, 6707−6732.
(40) Kummel, A. C.; Sitz, G. O.; Zare, R. N. Determination of Population, Alignment, and Orientation Using Laser Induced Fluorescence with Unresolved Emission. *J. Chem. Phys.* **1988**, *88*, 7357−7368.
(41) Hou, H.; Gulding, S. J.; Rettner, C. T.; Wodtke, A. M.; Auerbach, D. J. The Stereodynamics of a Gas-Surface Reaction. *Science* **1997**, *277*, 80−82.
(42) Nogueira, J. J.; Vazquez, S. A.; Mazyar, O. A.; Hase, W. L.; Perkins, B. G.; Nesbitt, D. J.; Martinez-Nunez, E. Dynamics of CO2 Scattering Off a Perfluorinated Self-Assembled Monolayer. Influence of the Incident Collision Energy, Mass Effects, and Use of Different Surface Models. *J. Phys. Chem. A* **2009**, *113*, 3850−3865.
(43) Martinez-Nunez, E.; Rahaman, A.; Hase, W. L. Chemical Dynamics Simulations of CO2 Scattering Off a Fluorinated Self-Assembled Monolayer Surface. *J. Phys. Chem. C* **2007**, *111*, 354−364.
(44) Isa, N.; Gibson, K. D.; Yan, T.; Hase, W.; Sibener, S. J. Experimental and Simulation Study of Neon Collision Dynamics with a 1-Decanethiol Monolayer. *J. Chem. Phys.* **2004**, *120*, 2417−2433.
(45) Yan, T.-Y.; Hase, W. L. Origin of the Boltzmann Translational Energy Distribution in the Scattering of Hyperthermal Ne Atoms Off a Self-Assembled Monolayer. *Phys. Chem. Chem. Phys.* **2000**, *2*, 901−910.
(46) Yan, T.-Y.; Hase, W. L.; Barker, J. R. Identifying Trapping Desorption in Gas-Surface Scattering. *Chem. Phys. Lett.* **2000**, *329*, 84−91.
(47) Day, B. S.; Shuler, S. F.; Ducre, A.; Morris, J. R. The Dynamics of Gas-Surface Energy Exchange in Collisions of Ar Atoms with Omega-Functionalized Self-Assembled Monolayers. *J. Chem. Phys.* **2003**, *119*, 8084−8096.
(48) Ulman, A. Formation and Structure of Self-Assembled Monolayers. *Chem. Rev.* **1996**, *96*, 1533−1554.
(49) Roscioli, J. R.; Bell, D. J.; Nelson, D. J.; Nesbitt, D. J. State-Resolved Velocity Map Imaging of Surface-Scattered Molecular Flux. *Phys. Chem. Chem. Phys.* **2012**, *14*, 4070−4080.
(50) Roscioli, J. R.; Nesbitt, D. J. Quantum State Resolved Scattering from Room-Temperature Ionic Liquids: The Role of Cation Versus Anion Structure at the Interface. *J. Phys. Chem. A* **2011**, *115*, 9764−9773.
(51) Squitieri, E.; Benjamin, I. Organic Monolayers as Mimics of Liquid/Liquid Interfaces: Molecular Dynamics Study of Electronic Spectra and Solvent Dynamics. *J. Phys. Chem. B* **2001**, *105*, 6412−6419.
(52) Love, J. C.; Estroff, L. A.; Kriebel, J. K.; Nuzzo, R. G.; Whitesides, G. M. Self-Assembled Monolayers of Thiolates on Metals as a Form of Nanotechnology. *Chem. Rev.* **2005**, *105*, 1103−1169.
(53) Roscioli, J. R.; Nesbitt, D. J. Quantum State Resolved Velocity-Map Imaging Spectroscopy: A New Tool for Collision Dynamics at Gas/Self-Assembled Monolayer Interfaces. *Faraday Discuss.* **2011**, *150*, 471−479.
(54) Proch, D.; Trickl, T. A High-Intensity Multi-Purpose Piezo-electric Pulsed Molecular-Beam Source. *Rev. Sci. Instrum.* **1989**, *60*, 713−716.
(55) Arepalli, S.; Presser, N.; Robie, D.; Gordon, R. J. Detection of Cl Atoms and HCl Molecules by Resonantly Enhanced Multiphoton Ionization. *Chem. Phys. Lett.* **1985**, *118*, 88−92.

DOI: 10.1021/acs.jpcc.6b03973
J. Phys. Chem. C 2016, 120, 16687−16698

(56) Green, D. S.; Bickel, G. A.; Wallace, S. C. (2 + 1) Resonance Enhanced Multiphoton Ionization of Hydrogen-Chloride in a Pulsed Supersonic Jet - Spectroscopic Survey. *J. Mol. Spectrosc.* **1991**, *150*, 303−353.
(57) Ashfold, M. N. R.; Nahler, N. H.; Orr-Ewing, A. J.; Vieuxmaire, O. P. J.; Toomes, R. L.; Kitsopoulos, T. N.; Garcia, I. A.; Chestakov, D. A.; Wu, S. M.; Parker, D. H. Imaging the Dynamics of Gas Phase Reactions. *Phys. Chem. Chem. Phys.* **2006**, *8*, 26−53.
(58) Eppink, A. T. J. B.; Parker, D. H. Velocity Map Imaging of Ions and Electrons Using Electrostatic Lenses: Application in Photoelectron and Photofragment Ion Imaging of Molecular Oxygen. *Rev. Sci. Instrum.* **1997**, *68*, 3477−3484.
(59) Townsend, D.; Minitti, M. P.; Suits, A. G. Direct Current Slice Imaging. *Rev. Sci. Instrum.* **2003**, *74*, 2530−2539.
(60) Barker, J. A.; Auerbach, D. J. Gas-Surface Dynamics, Velocity Distributions, Trapping and Residence Times. *Faraday Discuss. Chem. Soc.* **1985**, *80*, 277−289.
(61) McClelland, G. M.; Kubiak, G. D.; Rennagel, H. G.; Zare, R. N. Determination of Internal-State Distributions of Surface Scattering Molecules - Incomplete Rotational Accommodation of No on Ag(111). *Phys. Rev. Lett.* **1981**, *46*, 831−834.
(62) Cowin, J. P.; Yu, C. F.; Sibener, S. J.; Wharton, L. Hd Scattering from Pt(111) - Rotational-Excitation Probabilities. *J. Chem. Phys.* **1983**, *79*, 3537−3549.
(63) Lykke, K. R.; Kay, B. D. Rotationally Inelastic Gas-Surface Scattering - HCl from Au(111). *J. Chem. Phys.* **1990**, *92*, 2614−2623.
(64) Tamada, K.; Hara, M.; Sasabe, H.; Knoll, W. Surface Phase Behavior of N-Alkanethiol Self-Assembled Monolayers Adsorbed on Au(111): An Atomic Force Microscope Study. *Langmuir* **1997**, *13*, 1558−1566.
(65) Oron, A.; Davis, S. H.; Bankoff, S. G. Long-Scale Evolution of Thin Liquid Films. *Rev. Mod. Phys.* **1997**, *69*, 931−980.
(66) King, M. E.; Fiehrer, K. M.; Nathanson, G. M.; Minton, T. K. Effects of Thermal Roughening on the Angular Distributions of Trapping and Scattering in Gas-Liquid Collisions. *J. Phys. Chem. A* **1997**, *101*, 6556−6561.
(67) Phillips, L. F.; Nesbitt, D. J. A 'Hot-Spot' Model for Impulsive Scattering at the Gas-Liquid Interface. *Chem. Phys. Lett.* **2012**, *546*, 53−57.
(68) Minton, T. K.; Alexander, W. A.; Murray, V. J.; Shen, L.; Nathanson, G. M. Comparative Dynamics of O, Ar, and CO2 Scattering on Liquid and Self-Assembled Monolayer Surfaces. *Abstr. Pap. Am. Chem. Soc.* **2013**, *245*.
(69) Bagot, P. A. J.; Waring, C.; Costen, M. L.; McKendrick, K. G. Dynamics of Inelastic Scattering of OH Radicals from Reactive and Inert Liquid Surfaces. *J. Phys. Chem. C* **2008**, *112*, 10868−10877.
(70) Kohler, S. P. K.; Allan, M.; Costen, M. L.; McKendrick, K. G. Direct Gas-Liquid Interfacial Dynamics: The Reaction between O(3p) and a Liquid Hydrocarbon. *J. Phys. Chem. B* **2006**, *110*, 2771−2776.
(71) Rahaman, A.; Zhou, J. B.; Hase, W. Effects of Projectile Orientation and Surface Impact Site on the Efficiency of Projectile Excitation in Surface-Induced Dissociation: Protonated Diglycine Collisions with Diamond (111). *Int. J. Mass Spectrom.* **2006**, *249−250*, 321−329.
(72) Herzberg, G. *Electronic Spectra and Electronic Structure of Polyatomic Molecules*; Van Nostrand: New York, 1966.
(73) Thuo, M. M.; Reus, W. F.; Nijhuis, C. A.; Barber, J. R.; Kim, C.; Schulz, M. D.; Whitesides, G. M. Odd-Even Effects in Charge Transport across Self-Assembled Monolayers. *J. Am. Chem. Soc.* **2011**, *133*, 2962−2975.

DOI: 10.1021/acs.jpcc.6b03973
J. Phys. Chem. C 2016, 120, 16687−16698